New BIOTECHNOLOGY 84 (2024) 64–76

Contents lists available at ScienceDirect

New BIOTECHNOLOGY

journal homepage: www.elsevier.com/locate/nbt

Engineering the substrate specificity and regioselectivity of *Burkholderia thailandensis* lipoxygenase

Ruth Chrisnasari [a,b,c], Marie Hennebelle [a], Khoa A. Nguyen [a], Jean-Paul Vincken [a], Willem J.H. van Berkel [a], Tom A. Ewing [b,*]

[a] *Laboratory of Food Chemistry, Wageningen University & Research, Bornse Weilanden 9, 6708 WG Wageningen, the Netherlands*
[b] *Wageningen Food & Biobased Research, Wageningen University & Research, Bornse Weilanden 9, 6708 WG Wageningen, the Netherlands*
[c] *Faculty of Biotechnology, University of Surabaya (UBAYA), Surabaya 60293, Indonesia*

ARTICLE INFO

Keywords:
Dioxygenation
Hydroperoxide
Lipoxygenase
Fatty acid oxidation

ABSTRACT

Lipoxygenases (LOXs) catalyze the regioselective dioxygenation of polyunsaturated fatty acids (PUFAs), generating fatty acid hydroperoxides (FAHPs) with diverse industrial applications. Bacterial LOXs have garnered significant attention in recent years due to their broad activity towards PUFAs, yet knowledge about the structural factors influencing their substrate preferences remains limited. Here, we characterized a bacterial LOX from *Burkholderia thailandensis* (Bt-LOX), and identified key residues affecting its substrate preference and regioselectivity through site-directed mutagenesis. Bt-LOX preferred ω-6 PUFAs and exhibited regioselectivity at the ω-5 position. Mutations targeting the substrate binding pocket and the oxygen access channel led to the production of three active variants with distinct catalytic properties. The A431G variant bifurcated dioxygenation between the ω-5 and ω-9 positions, while F446V showed reduced regioselectivity with longer PUFAs. Interestingly, L445A displayed altered substrate specificity, favoring ω-3 over ω-6 PUFAs. Furthermore, L445A shifted the regioselectivity of dioxygenation to the ω-2 position in ω-3 PUFAs, and, for some substrates, facilitated dioxygenation closer to the carboxylic acid terminus, suggesting an altered substrate orientation. Among these variants, L445A represents a significant milestone in LOX research, as these alterations in substrate specificity, dioxygenation regioselectivity, and substrate orientation were achieved by a single mutation only. These findings illuminate key residues governing substrate preference and regioselectivity in Bt-LOX, offering opportunities for synthesizing diverse FAHPs and highlighting the potential of bacterial LOXs as biocatalysts with widespread applications.

Introduction

Lipoxygenases (LOXs; EC 1.13.11.x) are non-heme iron (or, in some cases, manganese) dependent enzymes that catalyze the regioselective dioxygenation of polyunsaturated fatty acids (PUFAs), leading to the formation of fatty acid hydroperoxides (FAHPs). This regioselective dioxygenation offers diverse applications in the food, chemical, and pharmaceutical industries, as the position of the hydroperoxide group in FAHPs determines the properties of the derived products. For instance, the combination of LOXs, which selectively add a hydroperoxide group at specific positions, with a hydroperoxide lyase can transform PUFAs into hemiacetals that spontaneously dissociate, yielding aldehydes of various lengths [1]. Different lengths of aldehydes and their derivative alcohols are valuable to the food and flavor industries. Moreover, different lengths of aldehydes offer advantages for producing various materials, including biobased polymers and a range of chemicals, as the chain length determines the properties of those materials [2–5]. LOXs with different regioselectivity can also be used for the production of di-

Abbreviations: LOX, lipoxygenase; PUFA, polyunsaturated fatty acid; LA, linoleic acid; ALA, α-linolenic acid; GLA, γ-linolenic acid; AA, arachidonic acid; EPA, eicosapentaenoic acid; DPA, docosapentaenoic acid; DHA, docosahexaenoic acid; 13-HPODE, 13-hydroperoxy-9*Z*,11*E*-octadecadienoic acid; 13-HPOTrE, 13-hydroperoxy-9*Z*,11*E*,15*Z*-octadecatrienoic acid; 15-HPETE, 15-hydroperoxy-5*Z*,8*Z*,11*Z*,13*E*-eicosatetraenoic acid; 12-HPEPE, 12-hydroperoxy-5*Z*,8*Z*,10*E*,14*Z*,17*Z*-eicosapentaenoic acid; 17-HPDPE, 17-hydroperoxy-7*Z*,10*Z*,13*Z*,15*E*,19*Z*-docosahexaenoic acid.

* Corresponding author.
E-mail addresses: ruth.chrisnasari@wur.nl (R. Chrisnasari), marie.hennebelle@wur.nl (M. Hennebelle), khoa.nguyen@wur.nl (K.A. Nguyen), jean-paul.vincken@wur.nl (J.-P. Vincken), willem.vanberkel@wur.nl (W.J.H. van Berkel), tom.ewing@wur.nl (T.A. Ewing).

https://doi.org/10.1016/j.nbt.2024.09.007
Received 17 June 2024; Received in revised form 9 September 2024; Accepted 25 September 2024
Available online 26 September 2024

and trihydroperoxy fatty acids, which can be further reduced to di- and trihydroxy fatty acids [6,7]. Di- and trihydroxy fatty acids, also referred to as specialized pro-resolving mediators, are of interest for pharmaceutical applications [8], as they are involved in the resolution of inflammation and infection [9,10]. Their broad industrial potential has prompted the exploration of new LOXs with different regioselectivity from various sources [8,11–16].

Among different sources of LOXs, bacterial LOXs have garnered increasing attention in the past few years due to their ability to act on a wide range of PUFAs, spanning chain lengths from C18 to C22 [11,13,15–18]. These bacterial LOXs also exhibit distinct substrate specificities. Certain bacterial LOXs, such as those from *Pseudomonas* sp. 42A2, *Burkholderia thailandensis*, *Calothrix* sp. HK-06, *Sphingopyxis macrogoltabida*, and *Myxococcus xanthus*, demonstrate pronounced activity towards linoleic acid (LA; C18:2), with lower activity towards α-linolenic acid (ALA; C18:3) [11,16,18–20]. Other bacterial LOXs from *Myxococcus fulvus* and *Pseudomonas aeruginosa* PAO1 prefer longer PUFAs, i.e., eicosapentaenoic acid (EPA; C20:5) and docosahexaenoic acid (DHA, C22:6), respectively [15,17]. Such variability in substrate specificity has also been observed in LOXs from other kingdoms [21]. Nevertheless, the underlying mechanisms behind the substrate specificities of LOXs remain poorly understood [1].

Besides having distinct substrate specificity, bacterial LOXs also exhibit distinct regioselectivities towards PUFAs [22]. For instance, *Pseudomonas aeruginosa* PAO1 LOX introduces a hydroperoxide group at the ω-5 position in C18 to C22 PUFAs, [17]. LOXs from *Cyanothece* sp. and *Acaryochloris marina* exhibit regioselectivity at the ω-6 position for ω-3 PUFAs (i.e., ALA and EPA) and at the ω-9 position for ω-6 PUFAs (i.e., LA and arachidonic acid (AA; C20:4)) [13,23]. LOXs from *Myxococcus xanthus* and *Myxococcus fulvus* target the ω-5 position on C18 PUFAs and the ω-8 position on C20 and C22 PUFAs. LOX from *Nostoc* sp. targets the ω-9 position on LA, ALA and AA [24]. *Sphingopyxis macrogoltabida* LOX has been shown to add a hydroperoxide group at the ω-9 position of C18 PUFAs (i.e., LA, γ-linolenic acid (GLA; C18:3)) and at the ω-11 position of C20 and C22 PUFAs (i.e., AA, EPA, docosapentaenoic acid (DPA; C22:5) and DHA) [12,18]. These facts indicate that the regioselectivity of LOXs is influenced by the chain length as well as the number and the position of double bonds of the fatty acid. Furthermore, the regioselectivity of LOXs is determined by the orientation of the substrate when entering the enzyme's substrate binding pocket. The fatty acid substrate can slide into the binding pocket either with its methyl-end (tail) or with its carboxyl-end (head) first. This concept was previously used to explain the regioselectivity of the double dioxygenation reactions of LOXs, such as 5,15-dioxygenation of AA as well as 7,17-dioxygenation of DPA and DHA [8,25,26]. In these double dioxygenation reactions, it seems that the substrate first enters the binding pocket in a certain orientation and undergoes dioxygenation to form an FAHP. Subsequently, this FAHP re-enters the binding pocket in the inverse orientation and is deoxygenated, yielding a dihydroperoxy fatty acid as the final product. These double dioxygenation reactions of LOXs demonstrated that the same enzyme is able to catalyze different regioselectivities, providing evidence that both tail-first and head-first binding can occur in the same active site.

In addition to being affected by the substrate's properties and orientation, the regioselectivity of LOX is also influenced by specific structural characteristics of the enzyme, including the depth of the substrate-binding pocket [27], as well as the position and size of the migration channel that transports molecular oxygen to the active site [28]. The depth of the binding pocket is determined by the residues that are present at the bottom of the pocket. When bulky amino acid residues are present at the bottom of the pocket, the substrate will slide into the tunnel in a more superficial way compared to when small amino acid residues are present. Investigations into mammalian LOXs indicate that amino acid residues present at the bottom of the pocket correspond to: (1) I417 and M418, referred to as the Sloane determinant [29], (2) F353 known as the Borngräber 1 determinant [30], and (3) I593 referred to as the Borngräber 2 determinant [31]. Additionally, a residue known as the Coffa site, which is present at the bottom of the oxygen migration channel, has been proposed to govern the regio- and enantioselectivity of LOXs by directing oxygen molecules to the active site [32]. This site is predominantly occupied by either alanine or glycine. When the larger alanine residue is present at this site, it promotes oxygenation to occur at one specific position. Conversely, when the smaller glycine residue is present, the migration channel becomes more spacious [33], thereby promoting the splitting of the oxygenation reaction to different positions.

Among characterized bacterial LOXs, *Burkholderia thailandensis* LOX (Bt-LOX) has the ability to act on various PUFAs and has demonstrated higher activity compared to commercial soybean LOX [20]. Bt-LOX introduces a hydroperoxide group at the ω-5 position when using LA as a substrate [20,34]. The high activity of Bt-LOX provides a significant advantage for its potential application as an industrial biocatalyst. However, to better harness this potential, further comprehensive characterization is required, e.g., of its substrate preference, its regioselectivity with different PUFA substrates, and identification of key residues determining those preferences. According to our previous studies on clustering and phylogenetic analyses of bacterial LOXs, Bt-LOX has been identified as a member of the most populous cluster among bacterial LOXs. This cluster comprises 282 out of a total of 613 identical protein group bacterial LOXs [22]. However, members within this cluster exhibit significant variation in the residues forming their Sloane and Borngräber determinants [22], suggesting a potential diversity in regioselectivity. Despite this variability, less than 3 % of the members of this cluster have been characterized [22]. Investigating the amino acid residues that determine substrate preference and regioselectivity in Bt-LOX is therefore of interest, as uncovering these residues may elucidate the key determinants of these properties within the largest group of bacterial LOXs.

Uncovering the key determinants is often pursued through site-directed mutagenesis in the active site, a common approach in enzyme engineering [35]. However, this method may yield unintended consequences, such as enzyme inactivation, reduced activity, or diminished thermostability [15,16,18,36]. Therefore, when employing site-directed mutagenesis to generate enzyme variants for further applications, it becomes imperative to thoroughly assess these potential effects. Evaluating these potential effects of mutagenesis ensures the development of enzyme variants that maintain or enhance desired functionalities, thus facilitating their effective utilization in various biotechnological applications.

In this study, we characterized the biochemical properties of Bt-LOX, performed site-directed active site mutations, and evaluated the impact of those mutations on the activity, overall structure, thermostability, iron load, substrate preference, and regioselectivity of the enzyme. We hypothesized that altering residues within the oxygen migration channel and at the bottom of the substrate binding pocket will influence the substrate preference and regioselectivity of the enzyme, while still maintaining or having only a minor detrimental effect on the activity and other biochemical characteristics of the enzyme. Therefore, we set out to explore the effect of modifying these residues by site-directed mutagenesis, both to enhance our understanding of molecular mechanisms determining substrate specificity and regioselectivity in bacterial LOX, and to facilitate the synthesis of diverse FAHPs from different PUFAs, thereby promoting the utilization of bacterial LOX as a biocatalyst in a wide range of applications.

Materials and methods

Materials

The gene encoding *Burkholderia thailandensis* lipoxygenase (Bt-LOX) (GenBank accession no. **ABC36974.1**) with codons optimized for expression in *Escherichia coli* was purchased from GenScript Biotech,

Rijswijk, The Netherlands. The gene was inserted between the *Nde*I and *Blp*I restriction sites in a pET-19b plasmid (Novagen, USA) (Fig. S1). A 10x His-Tag and a enterokinase site were included at the N-terminus of the enzyme to enable protein purification by metal affinity chromatography. Materials used for enzyme production and purification were obtained from the following sources: *E. coli* BL21(DE3) competent cells from Invitrogen, California, USA; Luria Bertani medium, pepstatin A and ampicillin sodium salt from Sigma-Aldrich, Missouri, USA; isopropyl β-D-1-thiogalactopyranoside (IPTG) from Duchefa Biochemie B.V., Haarlem, The Netherlands; BugBuster master mix and Ni-NTA His-bind resin from Millipore-Merck, Darmstadt, Germany; cOmplete mini EDTA-free protease inhibitor cocktail from Roche, Mannheim, Germany; VivaSpin from GE Healthcare, Buckinghamshire, UK.

Chemicals used for enzymatic assays and product analysis were sourced as follows: linoleic acid (LA; C18:2 Δ9*Z*,12*Z*), α-linolenic acid (ALA; C18:3 Δ9*Z*,12*Z*,15*Z*), γ-linolenic acid (GLA; C18:3 Δ6*Z*,9*Z*,12*Z*), arachidonic acid (AA, C20:4 Δ5*Z*,8*Z*,11*Z*,14*Z*), eicosapentaenoic acid (EPA, C20:5 Δ5*Z*,8*Z*,11*Z*,14*Z*,17*Z*), docosahexaenoic acid (DHA, C22:6 Δ4*Z*,7*Z*,10*Z*,13*Z*,16*Z*,19*Z*) were obtained from Nu-Chek Prep, Inc., Minnesota, USA. Fatty acid hydroperoxide standards 13(*S*)-hydroperoxy-9*Z*,11*E*-octadecadienoic acid (13-HPODE), 13(*S*)-hydroperoxy-9*Z*,11*E*,15*Z*-octadecatrienoic acid (13-HPOTrE), 15(*S*)-hydroperoxy-5*Z*,8*Z*,11*Z*,13*E*-eicosatetraenoic acid (15-HPETE), 12(*S*)-hydroperoxy-5*Z*,8*Z*,10*E*,14*Z*,17*Z*-eicosapentaenoic acid (12-HPEPE), and 17(*S*)-hydroperoxy-4*Z*,7*Z*,10*Z*,13*Z*,15*E*,19*Z*-docosahexaenoic acid (17-HPDHE), were obtained from Larodan, Solna, Sweden. Xylenol orange tetrasodium salt, iron(II) sulfate heptahydrate, cumene hydroperoxide, and perchloric acid were acquired from Sigma-Aldrich, Missouri, USA. Ethyl acetate, methanol absolute and acetonitrile, all in ULCMS grade were purchased from Biosolve B.V., Valkenswaard, The Netherlands.

Protein expression and purification

Recombinant *E. coli* BL21(DE3) carrying the pET-19b_Bt-LOX plasmid was grown in Luria Bertani medium at 37 °C with continuous shaking at 250 rpm. As a control for protein production, the empty pET-19b plasmid was also included. Upon reaching an optical density of 0.6 −0.8 at 600 nm (OD600), 0.5 mM IPTG was added, and the culture was further incubated at 16 °C with shaking at 150 rpm for 48 h. Subsequently, cells were harvested by centrifugation at 7000⨯*g* for 15 min at 4 °C and stored at −20 °C until protein purification.

To purify Bt-LOX, frozen cell pellets from a 200 mL culture were treated with a lysis solution. The lysis solution consisted of one Mini EDTA-free cOmplete protease inhibitor cocktail tablet and 1 μM pepstatin A dissolved in 10 mL of BugBuster Master Mix. After centrifugation at 16,000⨯*g* for 20 min at 4 °C to remove cell debris, the resulting supernatant was filtered through a 0.22 μm membrane filter. Purification was then carried out using a gravity flow column packed with 1 mL of Ni-NTA His-bind resin. Prior to sample application, the column was equilibrated with 10 column volumes (CV) of an equilibration buffer composed of 50 mM NaH_2PO_4, 300 mM NaCl, and 10 mM imidazole at pH 7.0. The filtered supernatant was applied to the column, followed by washing with 2 CV each of four washing buffers at pH 7.0, containing 50 mM NaH_2PO_4, 300 mM NaCl, and increasing concentrations of imidazole (20, 50, 100, and 150 mM, respectively). Elution of the purified enzyme was achieved using 4 CV of elution buffer at pH 7.0, containing 50 mM NaH_2PO_4, 300 mM NaCl, and 250 mM imidazole. Concentration and desalting of elution fractions were performed using a VivaSpin spin filter with a molecular weight cut-off of 10 kDa, and the enzyme was stored in 100 mM Bis-Tris-HCl Buffer at pH 6.0. Protein content was determined using the Bradford assay [37].

Determination of molecular mass and iron content

Molecular mass of the purified enzyme was determined by SDS-PAGE analysis under denaturing conditions using NuPAGE 10 % Mini Protein Gel (Invitrogen, USA). SeeBlue Plus2 pre-stained standard (Invitrogen, USA) was used as a molecular marker. The relative molecular mass of the native enzyme was determined by gel filtration chromatography using a Superdex 200 Increase 10/300 GL column (Cytiva, the Netherlands). The enzyme solution was applied to the column and eluted with 20 mM sodium phosphate buffer (pH 7.0) containing 150 mM NaCl at a flow rate of 0.75 mL.min^{-1}. The column was calibrated with thyroglobulin (669 kDa), ferritin (440 kDa), aldolase (158 kDa), conalbumin (75 kDa), and ovalbumin (43 kDa). To determine the void volume, the elution volume of blue dextran (2000 kDa) was used. The relative molecular mass of the enzyme was determined by comparing retention time of the purified Bt-LOX to the retention times of the reference proteins. The partition coefficient (K_{AV}) was calculated using Eq. (1) [38], where V_o is the void volume, V_t is the total volume of the column, and V_e is the elution volume.

$$KAV = \frac{Ve - Vo}{Vt - Vo} \quad (1)$$

To determine the iron content, 15 mL of the purified enzymes were stored in 100 mM Bis-Tris buffer pH 7.0, reaching a final concentration of 60.7, 78.9, 193.7 and 227.7 μg/mL for native, A431G, F446V and L445A, respectively. The iron content in the samples was measured using ICP-MS in duplicate (SGS Nederland B.V., Spijkenisse, the Netherlands). The iron load (%) was calculated by dividing the measured iron content (μmol/L) by the enzyme concentration (μmol/L) and then multiplying by 100.

PUFAs substrate preparation

Solubilized PUFAs were freshly prepared following a previously described method with slight modifications [39]. In a 10 mL volumetric flask, PUFA (LA, ALA, GLA, AA, EPA or DHA) was mixed with 12.5 μL of Tween-20 in 4 mL milli-Q water. Upon addition of 0.55 mL of 0.5 M NaOH, the mixture became clear. Milli-Q water was added to bring the volume to 10 mL, resulting in a final PUFA concentration of 4.33 mM.

LOX activity measurement using FOX assay

Throughout this study, the enzyme activity was determined using the ferrous-oxidized xylenol orange (FOX) assay. FOX reagent was prepared freshly according to the previously described method [40]. The xylenol orange reagent consisted of 2.0 mM ferrous sulphate, 0.29 mM xylenol orange tetrasodium salt and 440 mM perchloric acid in methanol/water (9:1). The enzymatic reactions comprised 30 μL of the substrate solution, 5 μL of native enzyme solution or 15 μL of enzyme variant solution, and 100 mM Bis-Tris buffer at pH 6.0 to the total volume of 500 μL, resulting in final concentrations of 260 μM substrate and 6 nM native enzyme or 18 nM enzyme variant. For the blank, the volume of enzyme solution was replaced by 100 mM Bis-Tris buffer pH 6.0. The reaction mixtures were then incubated for 5 min at room temperature (~20 °C). Subsequently, 30 μL of the samples and the blank were transferred to a 96-well microplate containing 150 μL FOX reagent and mixed gently to stop the reaction. The mixture was then incubated for 15 min at room temperature for color development. After 15-minute incubation, the absorbance of the samples was measured at 570 nm using a Spectramax ID3 multi detection plate reader (Molecular Devices, LLC., California, USA). The concentration of hydroperoxides produced during the enzymatic reaction was calculated using cumene hydroperoxide as a calibration standard. For the quantification of hydroperoxides derived from different PUFAs, correction factors were applied due to the varied responses of FAHPs in the FOX assay. The correction factors were calculated by dividing the molar extinction coefficient of cumene hydroperoxide by the molar extinction coefficient of the corresponding standard FAHP. Specifically, correction factors of 1.24 for HPODE, 1.29 for HPOTE, 1.40 for HPETE, 1.96 for HPEPE, and 1.80 for HPDHE were used [40]. One unit of enzyme activity (U) is defined as the amount of

enzyme that produces 1 μmol of hydroperoxide per minute. The specific activity of the enzyme, expressed in U/mg, was calculated by dividing the enzyme activity (U) by the amount of enzyme used in milligrams. The specific activity, considering only the holoenzyme, was also calculated by taking the iron load into account.

Determination of optimum conditions and stability of the enzyme

For determination of the pH optimum, the activity of native Bt-LOX was tested using LA as a substrate. The reactions were incubated at room temperature (~20 °C) in various buffers: 100 mM citrate at pH 3.0, 4.0, and 5.0; 100 mM Bis-Tris at pH 6.0 and 7.0; and 100 mM Tris-HCl at pH 8.0, 9.0, and 10.0. To assess pH stability, the native Bt-LOX was incubated in the corresponding buffer for 0 to 45 min at room temperature. Following incubation, the enzyme activity was measured in the same corresponding buffer using LA as the substrate at room temperature. The residual activity of the enzyme after incubation at a certain pH was used to evaluate the pH stability of the enzyme. For determination of the optimum temperature, the activity of native Bt-LOX was tested using LA as the substrate. The enzymatic reactions were conducted at different temperatures (i.e., 20, 30, 40, and 50 °C, respectively) in 100 mM Bis-Tris pH 6.0. To evaluate the thermostability, the enzyme was exposed to various temperatures (i.e., 20, 30, 40, and 50 °C, respectively) for 0 to 240 min prior the enzymatic assay. The enzymatic assay was done in the optimal pH buffer (100 mM Bis-Tris pH 6.0) using LA as the substrate at room temperature. The residual activity of the enzyme after incubation at a certain temperature was used to evaluate the thermostability of the enzyme. The experiments for determining optimum conditions and stability of the enzyme were conducted in triplicate. The acquired data were analyzed using the nonparametric Kruskal-Wallis test with a significance level set at $p < 0.01$ (SPSS Statistics 28.0, IBM Corp.).

Computational modelling and mutation design

The three-dimensional structure of Bt-LOX was modeled using Alphafold2 [41] with the casp14 settings. Initial determination of target residues for mutagenesis involved a multiple sequence alignment between the Bt-LOX sequence and sequences of other characterized LOXs. The multiple sequence alignment was conducted using Jalview 2.11.3.2 with MUSCLE default setting [42]. This alignment aimed to identify residues in Bt-LOX that correspond to the sites determining regioselectivity in other LOXs (i.e., Sloane determinant, Borngräber 1 and 2 determinants, as well as the Coffa site). Subsequently, the positions of these residues were predicted using the superimposition of the obtained Alphafold model of Bt-LOX and the crystal structure of *Pseudomonas aeruginosa* 42A2 (PDB: 5IR5, sequence identity 49.6 %). Mutations were designed based on the results of multiple sequence alignment and the superimposition of the Bt-LOX Alphafold model. The variants of Bt-LOX were prepared in the same way as described above for the native Bt-LOX using genes codon optimized for expression in *Escherichia coli* purchased from GenScript Biotech, Rijswijk, The Netherlands.

Circular Dichroism (CD) spectroscopy and thermal midpoint of unfolding determination

To assess how the mutations impact the overall structure and thermostability of Bt-LOX, CD spectroscopy was performed. The CD spectra of native Bt-LOX and the active site variants were recorded from 190 to 260 nm at initial condition and after 5 h of incubation at room temperature (~20 °C). The purified enzymes were diluted in 100 mM sodium phosphate buffer pH 6.0 to an approximate concentration of 100 μg/mL. Subsequently, 350 μL of each diluted enzyme solutions was transferred to a 1 mm-path length Quartz cuvette (Hellma analytics, Müllheim, Germany) and the CD spectra of the enzymes were measured using a Jasco J-1500 Circular Dichroism Spectrophotometer (Easton, USA).

To evaluate the effect of mutation on thermostability of the enzymes, native Bt-LOX and its variants were exposed to increasing temperatures. Generally, when a protein is exposed to increasing temperatures, it transitions from a folded state to an unfolded state. During this unfolding process, the protein may exist in one or more intermediate states, where it is partially unfolded, followed by a fully denatured state [43]. To understand the effect of increasing temperature on the unfolding process of Bt-LOX and its variants, the ellipticity (θ) at 220 nm as a function of the increasing temperature from 20 to 85 °C was measured. The wavelength of 220 nm was selected because it showed significant negative ellipticity, indicative for the helical structures of the folded state [44]. To calculate the thermal midpoint of unfolding (Tm) of Bt-LOX and its variants, a mathematical model was developed. This model describes the transition of ellipticity $\theta(T)$ of the protein at temperature T in two scenarios [45]. The first scenario involves a single transition between the folded and unfolded state, as described by Eqs. (2)–(4), in the case that Eq. (3) = 0 indicates no further transition step. The second scenario describes the transition from the folded state to the intermediate state and subsequently to the fully denatured state, following Eqs. (2)–(4). The fraction of protein transitioning from the folded to the intermediate state, observed as an exponential curve with a slower rate k_1, was quantitively expressed by the following Weibull function [45].

$$\alpha_1 = \frac{[\mathrm{I}]}{[\mathrm{F}]+[\mathrm{U}]} = \exp(-k_1 T^{n_1}) \tag{2}$$

The fraction of protein transitioning from the intermediate to the unfolded state, observed as an exponential curve with a faster rate k_2, was quantitatively expressed by the following Weibull function [45]:

$$\alpha_2 = \frac{[\mathrm{D}]}{[\mathrm{F}]+[\mathrm{U}]} = \exp(-k_2 T^{n_2}) \tag{3}$$

where [F] and [U] are the concentrations of proteins in the folded and the unfolded states at temperature T, respectively; [U] = [I] + [D], where [I] and [D] are the total concentration of proteins at intermediate state and fully denatured state at temperature T, respectively; k_1 is the rate of protein transition from the folded state to the intermediate state with an increase in T; k_2 is the rate of protein transition from the intermediate state to the fully denatured state with an increase in T; n_1 and n_2 are the shape factors, indicating the transition between two states. Ellipticity $\theta(T)$, which often starts with a slow rate increase followed by an exponential increase [43,44], was expressed for both scenarios in Eq. (4).

$$\theta(T) = (\theta_F + (\theta_{I1} - \theta_F)\alpha_1) + (\theta_{I2} + (\theta_D - \theta_{I2})\alpha_2) \tag{4}$$

where θ_F, θ_I, and θ_D designate the ellipticities of the protein at the folded state (i.e., the θ value at the initial temperature), intermediate state, and fully denatured state, respectively. Typically, the model calculates two separate kinetic curves for the transition from the folded to the intermediate state and from the intermediate to the fully denatured state [45]. In a simplified scenario, both the intermediate and the fully denatured states were considered as unfolded states (i.e., $\alpha_2 = 0$). In principle, θ_{I1} represent the maximum θ value of the first kinetic curve and θ_{I2} indicates the minimum θ value of the second kinetic curve. Since these θ_{I1} and θ_{I2} values cannot be directly determined from experiments, an optimization method was employed, as detailed below. The ratio between θ_{I2} and θ_{I1} indicates how quickly the intermediate state transitions to the fully denatured state.

To quantitatively describe the exponential curve of ellipticity $\theta(T)$ in Eq. (4), exponential equations were employed to describe α_1 and α_2 as outlined in Eqs. (2) and (3), respectively. These equations required the estimation of seven parameters: k_1 and k_2, n_1 and n_2, θ_{I1}, θ_{I2}, and θ_D. These estimates were derived by fitting Eqs. (2)–(4) to the experimental data of ellipticity $\theta(T)$ using a global optimization approach with the *'lsqnonlin'* algorithm of MATLAB 2021b software (Mathworks, Natick, MA, USA). The Root Mean Square Error (RMSE) values between the

experimental and numerical data were calculated to evaluate the model fitting. Ultimately, Tm was calculated at which the concentration of the enzyme in the folded state equals the concentration of the enzyme in the unfolded state, i.e., [F] = [U] = [I]+ [D] at Tm, and based on Eqs. (2) and (3) which yields $\alpha_1 + \alpha_2 = \frac{[I]+[D]}{[F]+[U]} = \frac{[U]}{[F]+[U]} = \frac{[U]}{2[U]} = 0.5$.

Determination of substrate preference

To determine the substrate preference of native Bt-LOX and its active site variants, the enzyme activity towards different PUFAs (LA, ALA, GLA, AA, EPA, or DHA) with a final concentration of 260 μM was determined using the FOX assay. The reactions were incubated at room temperature in 100 mM Bis-Tris buffer pH 6.0 and performed in six replicates. The acquired data were analyzed using the nonparametric Kruskal Wallis test with a significance level set at $p < 0.01$ (SPSS Statistics 28.0, IBM Corp.).

Analysis of regioselectivity of dioxygenation using RP-UHPLC-PDA-HRMS

Enzymatic reactions for the analysis of regioselectivity of dioxygenation consisted of 3 μg native Bt-LOX or 9 μg Bt-LOX variant, 240 μL of PUFA substrate (LA, ALA, GLA, AA, EPA, or DHA), and 100 mM Bis-Tris buffer pH 6.0 to a final volume of 1 mL, resulting in a final substrate concentration of 1.04 mM. Blank reactions for each substrate were prepared by dissolving the same amount of substrate in a total volume of 1 mL of 100 mM Bis-Tris buffer at pH 6.0. The mixture was then incubated for 30 min at room temperature with agitation at 300 rpm. Subsequently, the reaction mixture was transferred to a Kimax tube containing 5 mL of ethyl acetate and directly vortexed for a few seconds to stop the enzymatic reaction and extract the lipid fractions [16]. The mixture was centrifuged at 5000×*g* for 15 min at room temperature. After centrifugation, the mixture separated into three layers, i.e., aqueous bottom phase, denatured protein at the interlayer and organic upper phase. Afterwards, 4 mL of the upper layer were collected and evaporated by nitrogen flushing at 30 °C. Once the ethyl acetate had completely evaporated, the sample was diluted in 4 mL of methanol and stored at −80 °C until further analysis.

The enzymatic products were analyzed on a Thermo Vanquish UHPLC system (Thermo Fisher Scientific, Pittsburgh, PA, USA) equipped with a reversed-phase Acquity UPLC BEH C18 column (2.1×150 mm, 1.7 μm particle size; Waters Corporation, Milford, MA, USA) and coupled to a photodiode array detector (PDA) and a Thermo Q Exactive Focus Hybrid Quadrupole-Orbitrap Fourier Transform mass spectrometer (FTMS) (Thermo Fisher Scientific, Pittsburgh, PA, USA). The temperature at the autosampler was set to 10 °C. The flow rate was set at 350 μL min^{-1} and the column temperature was kept at 25 °C. The mobile phase A contained water:acetic acid (100:0.01, v/v) and mobile phase B consisted of acetonitrile:acetic acid (100:0.01, v/v). The elution program was set at 50 % B from 0 to 1.25 min, followed by a linear gradient to 90 % B from 1.25 to 51.43 min and to 100 % B from 51.43 to 52.68 min. The solvent composition was held at 100 % B from 52.68 to 58.90 min, followed by a decrease to 50 % B from 58.90 to 60.21 min. Finally, 50 % B was maintained from 60.21 to 66.48 min to allow for equilibration. The absorbance at 234 nm was monitored to detect the presence of conjugated diene moiety [46]. Additionally, accurate mass data was acquired with the high resolution mass spectrometer equipped with a Heated Electrospray Ionization (HESI) probe. The source conditions used in negative ionization mode were: capillary temperature of 250 °C, ion spray voltage of 2.5 kV, and 45 psi sheath gas flow rate. Full MS data were collected in discovery mode with resolution of 70,000 over the *m/z* range 250 to 1000. Higher-energy collisional dissociation (HCD) fragmentation data were also recorded using normalized collision energy of 35 % (when analyzing products from AA, EPA and DHA) and 45 % (when analyzing products from LA, ALA and GLA). Data were processed using Xcalibur 4.5 (Thermo). The identification of FAHPs involved analyzing peaks with specific masses corresponding to each PUFA. Additionally, the confirmation of these FAHP peaks was done by assessing their absorbance at 234 nm. The determination of the hydroperoxide position in FAHPs was conducted by examining specific fragments resulting from the cleavage of the C-C bond located near the hydroperoxide group [47,48]. The regioselectivity of the enzymes was determined by calculating the relative abundance of each FAHP using Eq. (5), while considering blank samples to mitigate for auto-oxidation products.

$$\text{Relative abundance}(\%) = \frac{(\textit{peak area of certain FAHP in sample} - \textit{peak area of certain FAHP in blank})}{(\textit{total peak area of FAHPs in sample} - \textit{total peak area FAHPs in blank})} \times 100\% \quad (5)$$

Molecular docking

To visualize the binding of substrates in the enzyme's binding pocket, molecular docking was performed using Molecular Operating Environment (MOE) version 2022.02 (Chemical Computing Group, Montreal, QC, Canada). The structures of PUFAs were obtained from PubChem to create a library in MOE. Structural preparation of PUFAs involved energy minimization and adjustment of protonation/deprotonation states. Before the docking process, iron was added to the Alphafold model of Bt-LOX. The position of the iron was confirmed by comparing the docking results to the position of the iron in *P. aeruginosa* LOX (PDB: 5IR5) (Fig. S2). The iron was then adjusted for valency, and the Bt-LOX-Fe structure was energy minimized and prepared by setting the pH to 6.0, ionic strength to 100 mM, and temperature to 25 °C. Determination of iron-coordinating residues was performed by selecting the corresponding residues that were found to be coordinated to iron in *P. aeruginosa* LOX (PDB: 5IR5, sequence identity 49.6 %). The prepared PUFAs were subsequently docked to the residues coordinating with iron (H388, H393, H565, N569, and I685) using triangle matcher placement and induced fit refinement settings. Scoring was based on London dG scoring, with a more negative S-score indicating increased binding affinity between PUFA and LOX. The docking process was conducted in triplicate, with each replicate collecting 30 poses, and the 5 poses with the lowest S-scores were evaluated. Docked poses were selected based on specific criteria, including the lowest S-score, Root Mean Square Deviation (RMSD) ≤ 2, and the proximity of the abstracted hydrogen's C-atom to iron.

Results and discussion

Biochemical properties of the native Burkholderia thailandensis LOX

Bt-LOX was purified from recombinant *E. coli* expressing the enzyme using Ni-NTA His-bind resin. The purified enzyme was obtained in soluble form and exhibited a single band in SDS-PAGE with an approximate molecular mass of 70 kDa (Fig. 1**A**). This value is similar to the theoretical mass of Bt-LOX (695 amino acids), including the enterokinase site and 10 histidine residues, which is 78.2 kDa. The protein was additionally analyzed by size exclusion chromatography (Fig. 1**B**), revealing that in 100 mM Bis-Tris pH 6.0, Bt-LOX predominantly exists as a

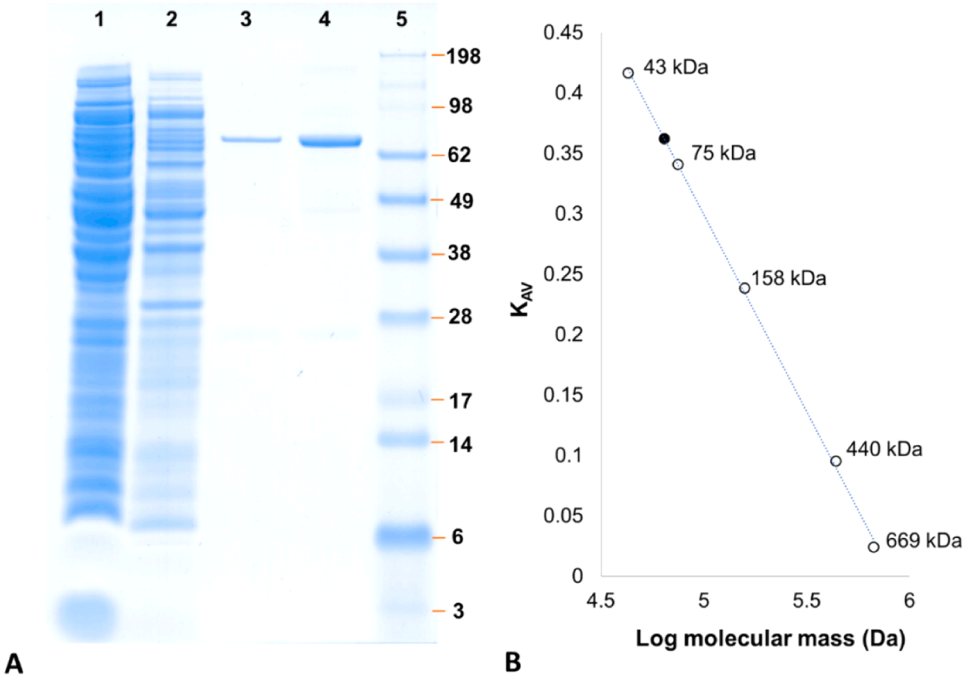

Fig. 1. SDS-PAGE analysis and molecular mass determination of the purified recombinant Bt-LOX. A. Lane 1: filtered supernatant of the cell lysate of *E. coli* expressing Bt-LOX. Lane 2: washing fraction obtained during column chromatography on Ni-NTA column. Lane 3: elution fraction obtained during column chromatography on Ni-NTA column. Lane 4: purified enzyme after concentrating and desalting. Lane 5: molecular mass marker proteins (the size of each protein (in kDa) is indicated in the figure). B. Determination of the relative molecular mass of purified native Bt-LOX using Superdex 200 Increase 10/300 GL size exclusion chromatography. The reference proteins are shown as open circles and Bt-LOX is shown as filled circle.

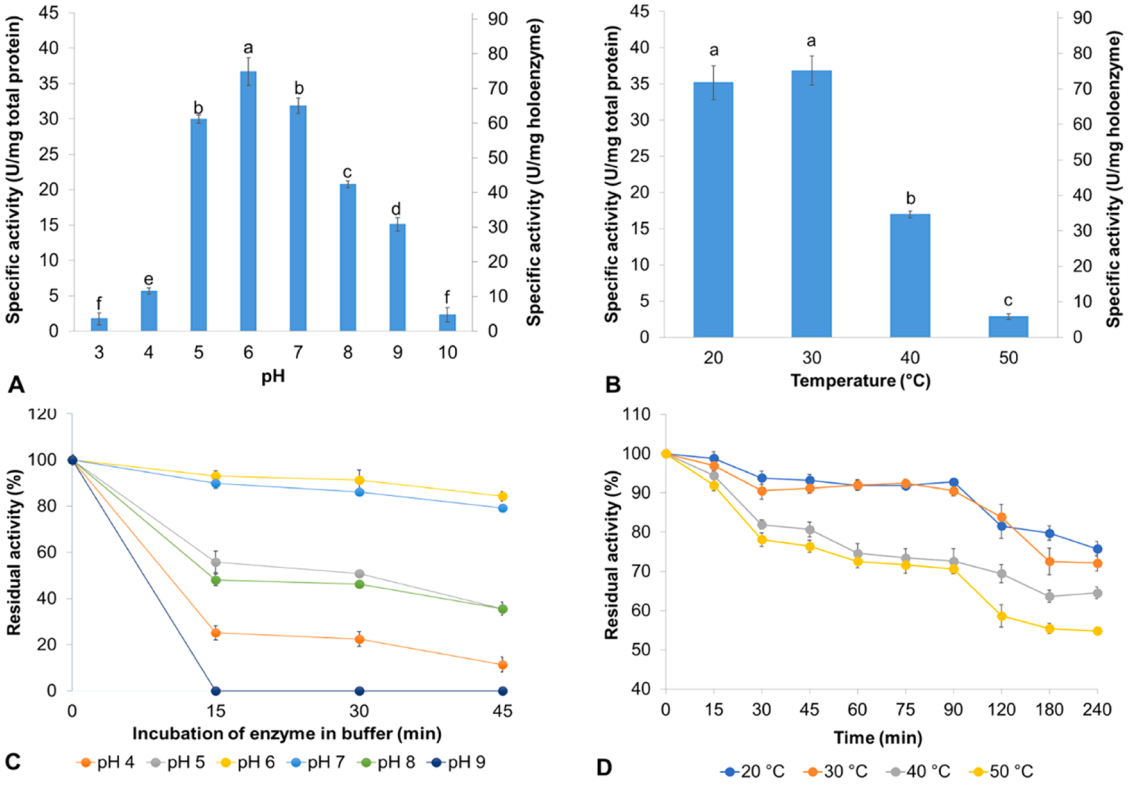

Fig. 2. Effect of pH and temperature on the activity and stability of Bt-LOX. The maximum activity of Bt-LOX was observed at pH 6.0 (A) and at a temperature of 20–30 °C (B). Bt-LOX showed highest stability at pH 6.0 (C) and a temperature of 20 °C (D). Data show mean ± SD ($n = 3$). Different letters indicate statistically significant differences at $p < 0.01$.

monomer. This predominantly monomeric state was consistently observed across enzyme concentrations ranging from 0.33 to 2.85 mg/mL (Fig. S3). However, minor quantities of dimeric, tetrameric, and higher oligomeric forms of the protein were also detected (Fig. S3). This finding contrasts with a previous report that described the enzyme as primarily in its dimeric form [20]. The disparity in the observed monomeric/dimeric states of the enzyme could be attributed to differences in ionic strength, buffer type, pH, and enzyme concentration used [49,50]. Since we used different buffer types, ionic strengths, and pH levels for dissolving the enzyme and for eluting it during gel filtration chromatography compared to the previous report [20], these factors may explain the difference in the observed monomeric/dimeric states of the enzyme.

The iron content of the purified Bt-LOX was measured by ICP-MS, revealing an iron load of 49 % (Table S1), indicating approximately half of the enzyme molecules have an iron atom present for utilization as a cofactor in their active site. However, the manganese content was not determined. Consequently, it cannot be ruled out that Bt-LOX may be partially loaded with manganese, as observed in some other bacterial LOXs [16,51]. Comparable iron loads were observed in other bacterial LOXs from *Cyanothece* sp. and *Pseudomonas aeruginosa*, with a percentage of 45 % and 67 %, respectively [51,52]. In contrast, the bacterial LOX from *Myxococcus fulvus* exhibited a much lower iron load of 6 % [15], while that from *Myxococcus xanthus* showed an iron load of 92 % [16]. The variation in iron-to-protein ratios among overexpressed bacterial LOXs may be attributed to differences in overexpression systems and conditions, as well as variations in 3D structure of the enzyme leading to differences in iron affinity.

The impact of pH and temperature on Bt-LOX activity and stability was assessed using LA as a substrate. Bt-LOX displayed its highest activity at pH 6.0 within the tested pH range of 3.0 to 10.0 at room temperature (Fig. 2A). To confirm whether pH 6.0 is optimal for all PUFAs, the activity of Bt-LOX on different PUFAs (LA, ALA, GLA, AA, EPA, and DHA) was measured across various buffers from pH 3.0 to 10.0 (Fig. S4). The results confirmed that pH 6.0 is indeed optimal for all tested PUFAs. Previous reports suggested that Bt-LOX is optimally active at pH 7.5 within the pH range of 6.5 to 8.5 tested [20]; however, our observation of a slightly different optimum pH may be attributed to the use of different buffer types and strength as well as the broader pH range evaluated. Bt-LOX exhibited its highest activity at temperatures between 20–30 °C (Fig. 2B). This result is consistent with previous reports suggesting that the enzyme is optimally active at temperatures between 25–30 °C [20]. In addition to the optimal conditions, the enzyme exhibited maximum stability at pH 6.0 and a temperature of 20 °C (Fig. 2C, D)).

Determination of amino acid residues potentially responsible for substrate preference and regioselectivity

To determine which amino acid residues might be responsible for substrate preference and regioselectivity in Bt-LOX, a multiple sequence alignment of Bt-LOX and other characterized LOXs was first performed.

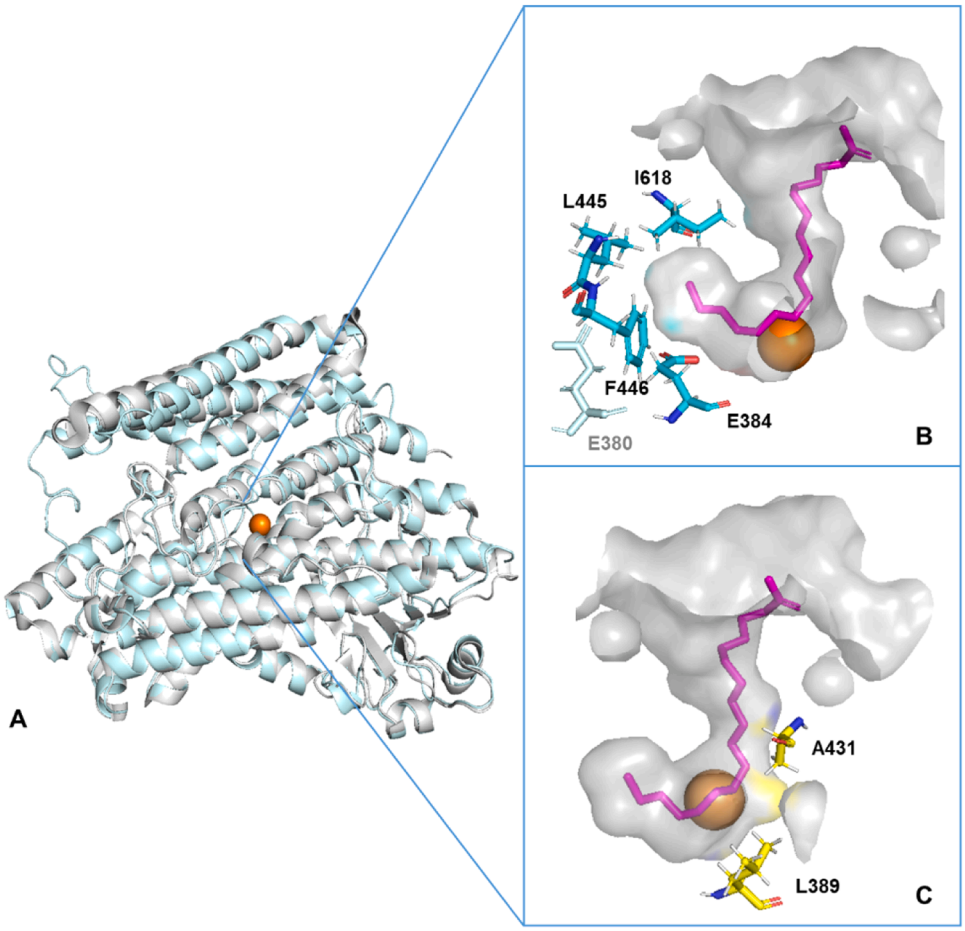

Fig. 3. Alphafold model for the structure of Bt-LOX. A. Superimposition of the Alphafold model of Bt-LOX shown in cyan and the crystal structure of *Pseudomonas aeruginosa* 42A2 shown in grey (PDB: 5IR5, sequence identity to Bt-LOX 49.6 %). The iron atom is shown as an orange sphere. B. Selected residues for binding pocket enlargement in Bt-LOX are indicated in cyan and the unselected residue indicated in pale cyan. The surface structure in grey indicates the substrate-binding pocket. The sn-2 fatty acid alkyl chain of a co-crystalized phospholipid which fills the substrate-binding channel in the *P. aeruginosa* 42A2 crystal structure is shown as magenta sticks. C. Residues of Bt-LOX selected for oxygen channel enlargement (in yellow).

This alignment unveiled residues in Bt-LOX that correspond to the sites determining regioselectivity in other LOXs (Fig. S5). Specifically, L445 and F446 corresponded to the Sloane determinant, A431 corresponded to the Coffa site, and E380 and I618 corresponded to the Borngräber determinants 1 and 2, respectively. The positions of these residues within the substrate binding pocket were predicted using the superimposition of the Alphafold model of Bt-LOX and the crystal structure of *Pseudomonas aeruginosa* 42A2 LOX (Fig. 3A). The superimposition was conducted with *Pseudomonas aeruginosa* 42A2 LOX because this enzyme belongs to the same bacterial LOX cluster as Bt-LOX, as determined by our previous bioinformatic analysis [22]. This superimposition confirmed the localization of L445, F446 and I618 at the bottom of the substrate binding pocket (Fig. 3B). However, E380 was observed to be less close to the pocket. Thus, E384 that was closer to the bottom of the binding pocket was selected instead. Additionally, A431 was located near the putative oxygen migration channel, as was L389, which was added to the list of residues of potential interest (Fig. 3C). All selected residues were subsequently replaced with smaller residues, as detailed in Table S2. Additionally, combinations of double, triple, and quadruple mutations on residues present at the bottom of the pocket were performed to assess the effect of further enlarging the substrate binding pocket (Table S2). Despite, all corresponding variants being successfully produced in soluble form and purified, only three variants showed activity: A431G, F446V, and L445A. The SDS-PAGE results displayed for each of these variants a single protein band with an approximate molecular mass of 70 kDa, similar to the native enzyme (Fig. S6). These variants were then used for further analysis.

Effect of the mutations on the thermostability and the iron load

Mutagenesis can lead to unintended outcomes, such as alterations in overall structure, reduced thermostability, or even enzyme inactivation [15,16,18,36]. Therefore, it is essential to thoroughly evaluate these potential effects when developing enzyme variants for further applications. To evaluate the impact of the mutations on the overall structure and thermostability of Bt-LOX, CD spectroscopy was conducted. The CD spectra of the enzyme variants closely resembled those of the native enzyme, even after a 5-hour incubation at room temperature (Fig. S7). These findings suggest that the mutations did not significantly alter the overall structure of Bt-LOX. To assess how the mutations influenced the thermostability of the enzymes, the ellipticity at 220 nm was measured as a function of temperature. At this wavelength, significant negative ellipticity and high signal-to-noise ratio were observed (Fig. S8). The results displayed in Fig. 4 indicate a sharp loss in negative ellipticity at 220 nm upon protein unfolding, suggesting a transition from helical structure at lower temperatures to a more random structure at higher temperatures.

The model describing a single transition between the folded and the unfolded state fitted poorly with the datasets (all RMSEs > 0.5). However, the model that describes the transition between the folded state to the intermediate state and subsequently to the fully denatured state fitted well with the experimental data (Fig. 4, RMSE ranging from 0.16 to 0.33). Thus, in our current study, the model described by Eqs. (2)–(4) was employed to calculate Tm. Fitting model parameters were derived and estimates of seven parameters are provided in Table S3 (i.e., k_1 and k_2; n_1 and n_2; θ_{I1}, θ_{I2}, and θ_D). By substituting estimates (Table S3) into $\alpha_1 + \alpha_2 = 0.5$, the Tm of each enzyme variant was calculated, yielding

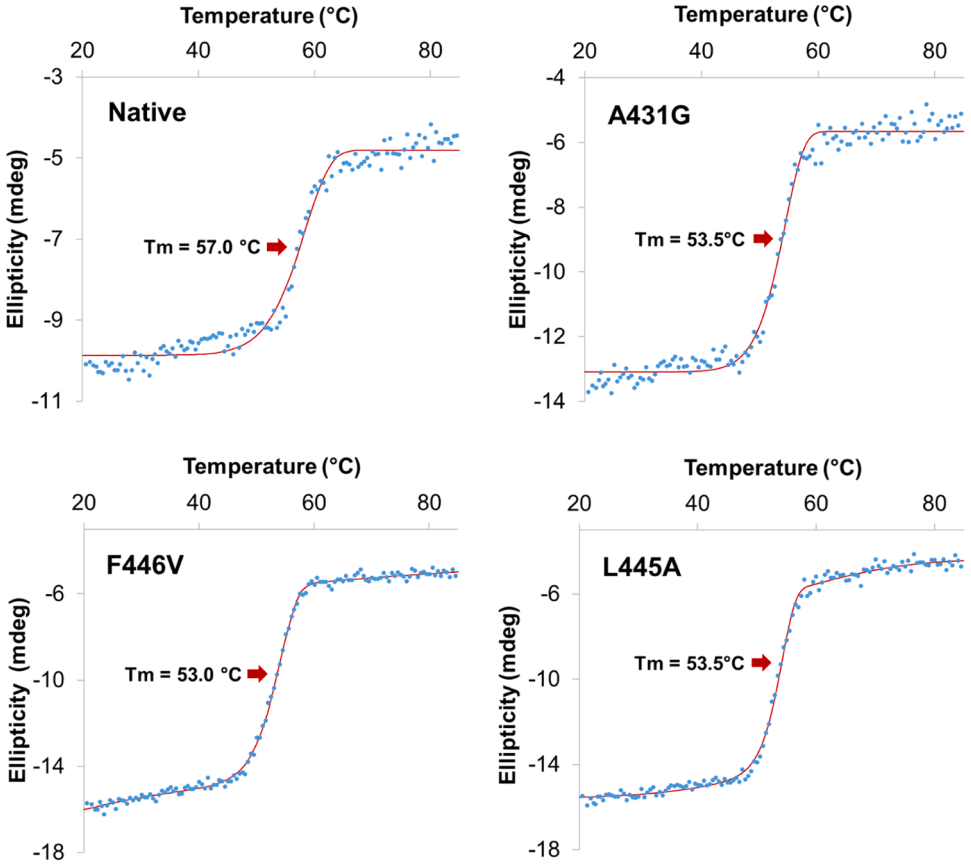

Fig. 4. Circular Dichroism (CD) thermal melting data of native Bt-LOX and its variants A431G, F446V, and L445A (shown in blue dots). To determine the thermal midpoint of unfolding (Tm), the ellipticity was monitored at 220 nm as a function of temperature. These figures illustrate that upon raising the temperature, the negative ellipticity of the folded protein gradually is lost with a sharp transition around the melting temperature (Tm). The Tm of each enzyme variant was calculated based on the fitting model (shown in red line).

values of 57.0 °C for the native, 53.5 °C for A431G, 53.0 °C for F446V, and 53.5 °C for L445A. These results indicate that the introduced mutations had only a slight impact on the enzyme's thermostability.

To assess the impact of mutations on the iron load of Bt-LOX, the iron content was measured using ICP-MS. The results, as detailed in Table S1, revealed that A431G exhibited an iron content similar to that of the native enzyme (49 %). However, both F446V and L445A exhibited slightly lower iron content compared to the native enzyme at 30 % and 41 %, respectively. These findings suggest that enlarging the bottom of the binding pocket had a more pronounced effect on altering the enzyme's iron load than enlarging the oxygen access channel. This enlargement may have affected the overall shape of the pocket, leading to a shift in the position of residues coordinating with the iron and consequently influencing the enzyme's iron load.

Effect of the mutations on the substrate preference and regioselectivity

To assess the impact of the mutations on the substrate specificity of Bt-LOX, enzyme activities were tested against PUFAs with varying chain lengths (C18 to C22), as well as different numbers (2 to 6) and positions (ω-3 and ω-6) of double bonds. The results revealed that the substrate preference of native Bt-LOX is influenced by the length of the PUFAs, along with the number and position of the double bonds (Fig. 5). Increasing the chain length and the number of double bonds (within the same ω position class) led to an increased activity of native Bt-LOX, as evidenced by the increasing activity towards AA (C20:4 ω-6) compared to LA (C18:2 ω-6) and towards DHA (C22:6 ω-3) compared to EPA (C20:5 ω-3) and ALA (C18:3 ω-3). The effect of increasing the number of double bonds was also observed in PUFAs with the same chain length, i.e., higher activity towards GLA (C18:3 ω-6) compared to LA (C18:2 ω-6). Additionally, the position of double bonds within the same carbon chain length influenced the substrate preference, as demonstrated by the increased enzyme activity towards GLA (C18:3 ω-6) compared to ALA (C18:3 ω-3). Altogether, native Bt-LOX exhibited a preference for longer and more unsaturated PUFAs, as well as for ω-6 PUFAs compared to ω-3 PUFAs. This preference aligns with observations made in *P. aeruginosa* LOXs [17,19,53], enzymes sharing similar residue sizes of their Sloane, Borngräber, and Coffa determinants with Bt-LOX [22]. However, these findings contrast with a previous report indicating that Bt-LOX exhibited significantly lower activity towards GLA compared to ALA, LA, or AA [20].

The A431G variant and the F446V variant showed a comparable substrate preference pattern as the native enzyme, although both variants were less active (Fig. 5). The biggest change in substrate specificity was observed for the L445A variant. Compared to the native enzyme, the L445A variant demonstrated a pronounced preference for ω-3 and longer PUFAs, while displaying a very low activity towards all tested ω-6 PUFAs (Fig. 5). These findings indicated that L445 plays an important role in determining the substrate preference of the enzyme. Alteration of substrate preference due to introduction of a smaller residue at the bottom of the binding pocket of LOX has not been reported before. This finding may open the opportunity to steer the substrate preference of the enzyme, thereby promoting the utilization of LOXs for derivatization of various PUFAs.

The evaluation of the impact of the mutations on the specific activities of the enzyme revealed notable differences. The specific activities of

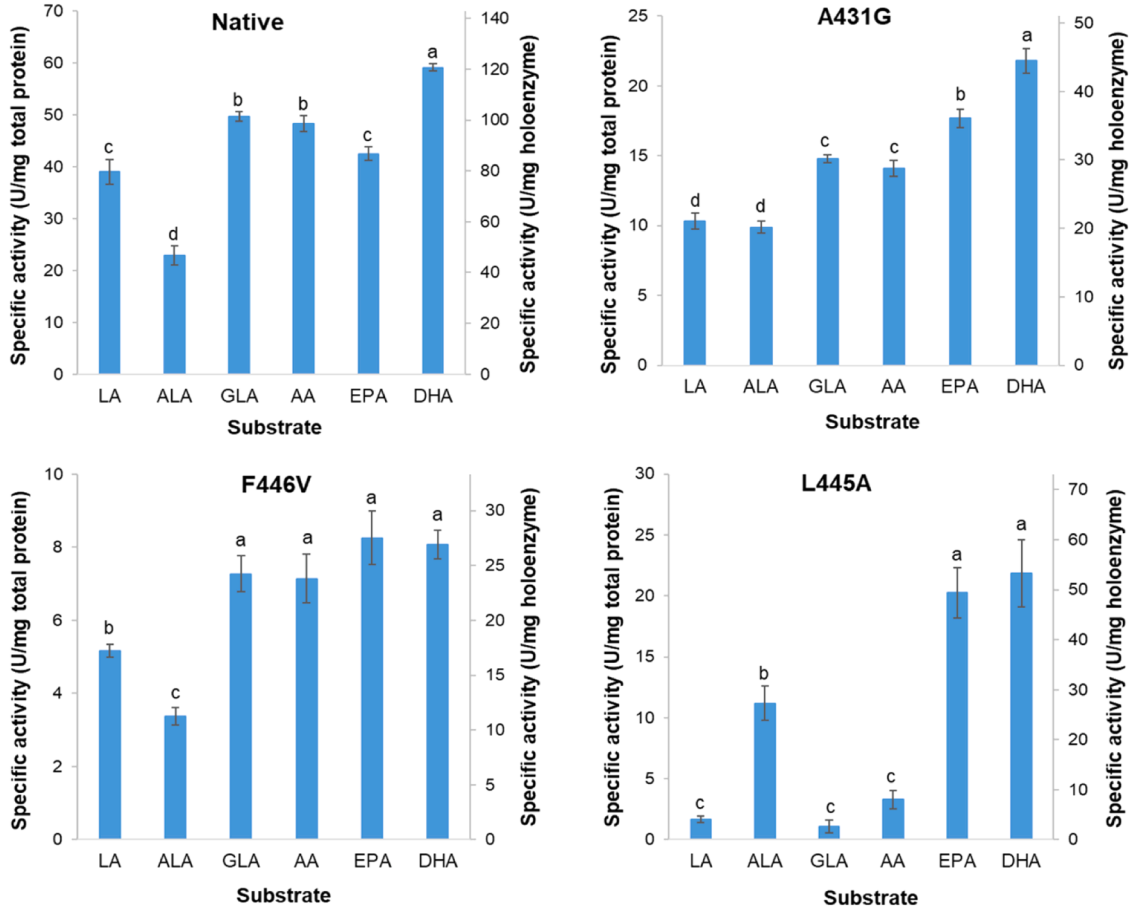

Fig. 5. Substrate preference of native Bt-LOX and its variants A431G, F446V and L445A. Six PUFA substrates were evaluated: linoleic acid (LA; C18:2 ω-6), α-linolenic acid (ALA; C18:3 ω-3), γ-linolenic acid (GLA; C18:3 ω-6), arachidonic acid (AA; C20:4 ω-6), eicosapentaenoic acid (EPA; C20:5 ω-3), and docosahexaenoic acid (DHA; C22:6 ω-3). Data are reported as mean ± SD ($n = 6$). Different letters indicate statistically significant differences at $p < 0.01$.

the L445A (specifically on ω-3 PUFAs) and A431G variants were approximately 3-fold lower compared to the native enzyme, while the F446V variant exhibited an approximately 6-fold decrease (Fig. 5). The decreased specific activity of the F446V and L445A variants may partly be due to their lower iron load compared to the native enzyme (Table S1). However, the decreased specific activity in the A431G variant, which has the same iron load as the native enzyme (Table S1), indicates that factors beyond the iron load play a role in determining specific activity. Comparable reductions in specific activity, ranging from 3- to 10-fold, have been reported for active site variants in other LOXs, such as those from *Sphingopyxis macrogoltabida*, *Cyanothece* sp., and *Myxococcus xanthus* [16,18,54]. Despite these reductions, the specific activities of the Bt-LOX variants remain within the range typically seen in bacterial LOXs (i.e., 5 to 30 U/mg) [22], suggesting a comparable specific activity of these variants relative to other bacterial LOXs.

To evaluate how the mutations affect the regioselectivity of the enzyme, RP-UHPLC-PDA-HRMS was used to determine the positions of hydroperoxide incorporation into the various PUFA substrates. The retention time of the resulting FAHPs, their relative abundance and their specific fragments in MS^2 spectra used for regioselectivity determination are listed in Table S4. Examples of the chromatograms and fragmentation patterns of FAHPs are given in Fig. S9 and Fig. S10, respectively.

Native Bt-LOX displayed a strong preference for dioxygenation at the ω-5 position in all tested PUFAs (Fig. 6). This preference indicated that the substrates enter the enzyme's binding pocket by their methyl-end first, as confirmed by the docking results in Fig. S11. The docking parameters of each selected docking pose are presented in Table S5. A strong preference for dioxygenation at the ω-5 position aligns with a previous report indicating that Bt-LOX introduces a hydroperoxide group at the ω-5 position when using LA as a substrate [20]. Regioselectivity preference at the ω-5 position has also been reported in *Pseudomonas aeruginosa* LOXs that belong to the same cluster and share similar residue sizes of their Sloane, Borngräber, and Coffa determinants with Bt-LOX [17,22,55,56]. These results suggest that bacterial LOXs residing in the same cluster of the phylogenetic tree and having the same size of residue on their specificity determinants, indeed have the same regioselectivity. Additionally, Bt-LOX exhibited some degree of activity towards the ω-2 position (i.e., in EPA and DHA), as well as towards positions closer to the carboxylic moiety (i.e., GLA, AA, and DHA). The latter results suggest that although there is a clear preference towards the entrance of the substrate with its methyl-end first, the binding pocket of native Bt-LOX is spacious enough to allow some carboxyl-end first orientation as also confirmed by the docking studies (Table S5).

Product analysis of A431G showed a splitting of the dioxygenation reaction between the ω-5 and ω-9 positions in almost all tested fatty acids. The split regioselectivity of the A431G variant of Bt-LOX confirms that this residue plays a crucial role in determining the regioselectivity of Bt-LOX. Possibly, the alanine residue present at this site in the native enzyme partially covers the oxygen migration channel and promotes oxygenation mostly at the ω-5 position (Fig. 7A left panel). However, in the A431G variant, the migration channel becomes more spacious, thereby promoting bifurcated oxygenation at both the ω-5 and ω-9

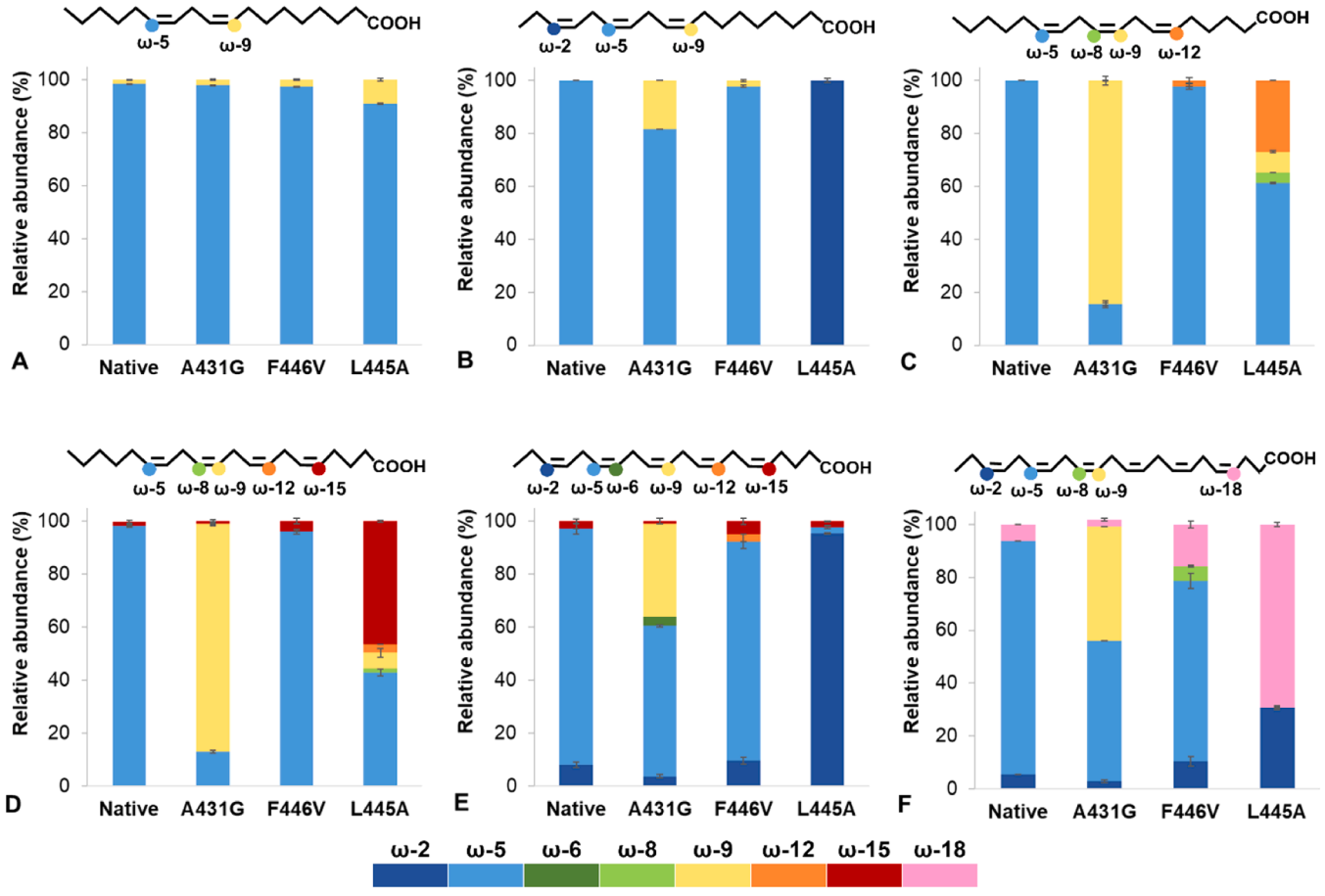

Fig. 6. Regioselectivity of dioxygenation of native Bt-LOX and its active site variants with different fatty acid substrates. The position of dioxygenation is counted from the methyl end (omega nomenclature). Different color indicates different position of hydroperoxide. Six different PUFAs were used and their structures are depicted above the bar charts with their oxidation sites labeled according to the respective omega positions: A. Linoleic acid (LA; C18:2 ω-6); B. α-linolenic acid (ALA; C18:3 ω-3); C. γ-linolenic acid (GLA; C18:3 ω-6); D. Arachidonic acid (AA; C20:4 ω-6); E. Eicosapentaenoic acid (EPA; C20:5 ω-3); F. Docosahexaenoic acid (DHA; C22:6 ω-3). Data are reported as mean ± SD of two biological replicates.

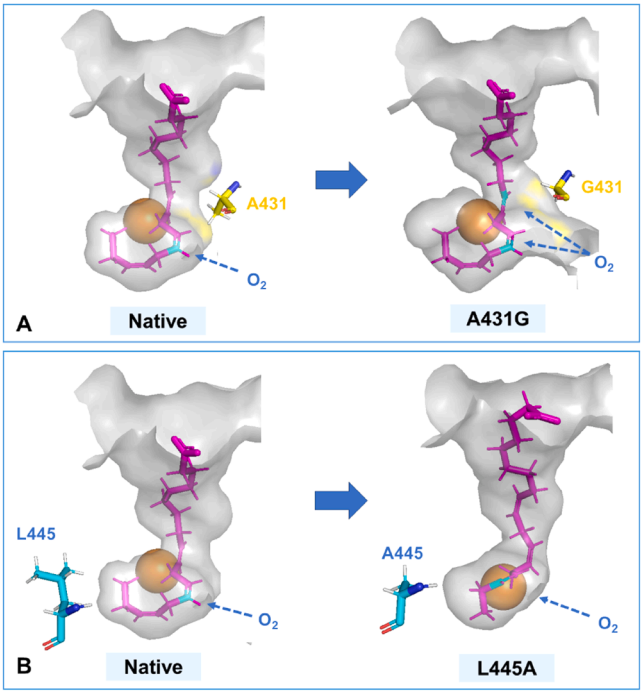

Fig. 7. The effects of mutations on the oxygen migration channel and substrate-binding pocket. A. The A431G substitution enlarges the oxygen channel, facilitating oxygen direction splitting (shown by blue dashed arrows) and enabling oxygenation to occur at both the ω-5 and ω-9 positions (highlighted in cyan). B. The L445A substitution changes the shape of the binding pocket, influences the penetration of the substrate, and leads to the shifting of oxygenation from the ω-5 to the ω-2 positions in ω-3 PUFAs (highlighted in cyan). The α-linolenic acid (ALA; C18:3 Δ9*Z*,12*Z*,15*Z*), shown in magenta, was docked to the Alphafold model of Bt-LOX using MOE 2022.02. Prior to the docking process, the iron atom (shown as an orange sphere) was added to the Alphafold model of Bt-LOX. The surface structure in grey indicates the substrate-binding pocket of Bt-LOX.

positions, as simulated by the docking result (Fig. 7A right panel). A similar effect of substituting the residue at the Coffa site with a smaller one has been reported for LOX from *Pseudomonas aeruginosa* [33]. In other LOXs, this effect was not always observed when changing the Coffa site residue into a smaller one. For instance, in *Oscillatoria nigroviridis* LOX, changing the residue in the Coffa site from alanine to glycine shifted the regioselectivity from the ω-5 position exclusively to the ω-9 position [57]. On the other hand, changing the residue in the Coffa site from alanine to glycine in *Myxococcus fulvus*, *Nostoc* sp., and *Anabaena* sp. PCC 7120 LOX did not affect the regioselectivity of the enzyme, while changing it to a bigger residue did [15,24,58]. It seems that in these enzymes, alanine is not sufficiently bulky to achieve the effect of narrowing the oxygen channel.

Similar to the native enzyme, F446V displayed a strong preference for dioxygenation at the ω-5 position in all tested PUFAs. However, F446V became slightly less regioselective with longer fatty acids containing a higher number of double bonds (i.e., with EPA and DHA) (Fig. 6). Additionally, with longer substrates, F446V demonstrated a slightly increasing level of dioxygenation at positions closer to the carboxylic acid group. These results suggest that residue F446 does not play a significant role in determining the regioselectivity of the enzyme. Similarly, no change in regioselectivity was observed after substituting residues in the Sloane determinant with smaller ones in *Myxococcus fulvus* LOX [15]. However, these results contrast with observations in mammalian 15-LOX, where substituting the corresponding residue with a smaller one (M418V) altered the enzyme's regioselectivity from exclusively ω-5 position to an equal mixture of ω-5 and ω-8 positions [29].

On the other hand, mutation of L445, the other residue that forms part of the Sloane determinant, into A445, caused a significant alteration in regioselectivity. The L445A variant demonstrated a shift in the preferred position of dioxygenation from the ω-5 to the ω-2 carbon atom for ω-3 PUFAs (Fig. 6), while maintaining its regioselectivity for ω-6 PUFAs mainly at the ω-5 position. The remaining regioselectivity for ω-6 PUFAs makes sense, as ω-5 is already the first position from the methyl end where dioxygenation can occur. The shift in regioselectivity toward the methyl end also explains why the activity of this variant is much lower towards ω-6 PUFAs, as the most preferred position for dioxygenation is not available in ω-6 PUFAs, resulting in lower activity towards less preferred positions. Furthermore, the shift in regioselectivity toward the methyl-end implies that ω-3 PUFAs penetrate less deeply into the substrate binding pocket.

The shift in regioselectivity toward the methyl-end in L445A is unexpected, as the mutation of L445 into a smaller residue was predicted to extend the bottom of the binding pocket. Generally, a shift towards the methyl-end regioselectivity has been demonstrated when introducing a larger residue into the binding pocket, making it more constrained and causing the substrate to enter the pocket more superficially [16,18,30]. Conversely, a shift in regioselectivity closer to the carboxyl-end was observed in other bacterial and mammalian LOXs when introducing a smaller residue into the binding pocket [8,29–31]. In another case, introducing a smaller residue into the binding pocket led to a loss in regioselectivity, resulting in the introduction of hydroperoxide groups at more random positions on the fatty acid [16]. However, according to the molecular docking simulation (Fig. 7B right panel), it appears that the substitution of L445A alters the position of other residues in the bottom of the binding pocket, affecting its shape and size, and making it smaller (Fig. S12). This alteration subsequently influences the substrate's penetration depth, leading to a shift in oxygenation closer to the methyl-end. The alteration in the binding pocket's shape resulting in a smaller pocket was also observed when using different ω-3 PUFAs (Fig. S13), confirming the shift in regioselectivity closer to the methyl-end in other ω-3 PUFAs.

The shift in regioselectivity from the ω-5 to the ω-2 carbon atom in L445A represents a significant milestone in LOX research, as regioselectivity at the ω-2 position has not been previously reported. Oxygenation of PUFAs at the ω-2 position is particularly interesting, as the resulting ω-2 FAHPs can potentially be converted into derivative products with properties distinct from those generated by the native enzyme. For instance, ω-2 FAHPs can be transformed into hemiacetals by hydroperoxide lyase, which decompose into aldehydes and oxo-fatty acids [59,60]. These oxo-fatty acids can then be further converted into ω-hydroxycarboxylic acids by alcohol dehydrogenase [61]. In addition to enzymatic transformation, the decomposition of FAHPs into oxo-fatty acids, followed by their reduction to ω-hydroxycarboxylic acids, can also be achieved through chemical methods [62,63]. This derivatization process enables the conversion of ω-2 FAHPs into longer-chain ω-hydroxycarboxylic acids than those produced by the native enzyme (Fig. S14). The utilization of these long-chain ω-hydroxycarboxylic acids could facilitate the production of various materials, such as bio-based polymers and a range of chemicals and intermediates, potentially with different properties than those derived from the ω-hydroxycarboxylic acids generated by native enzyme [2,64,65].

Intriguingly, the L445A variant exhibited a higher degree of dioxygenation at positions closer to the carboxyl end compared to the native enzyme when GLA, AA, and DHA were used as substrates (Fig. 6). These findings suggest that the L445A substitution in Bt-LOX promotes substrate entry via a carboxyl-end-first orientation, as also shown by the

docking results presented in Fig. S13B. While the concept of replacing the Sloane determinant with a smaller residue, leading to a shift in regioselectivity, is well-established, the impact of this mutation on changing substrate entrance orientation has not been previously reported. These results indicate that residue L445 plays a significant role in determining not only substrate specificity and regioselectivity, but also substrate orientation.

Conclusions

Mutations at the bottom of the substrate binding pocket and in the oxygen migration channel in Bt-LOX can impact its substrate preference and the regioselectivity of dioxygenation. The A431G substitution promoted the bifurcation of oxygen insertion to the ω-5 and ω-9 positions. The L445A replacement shifted the substrate specificity of the enzyme from ω-6 to ω-3 PUFAs. Substitution of this residue opens opportunities to steer the substrate preference of the enzyme. The L445A substitution also facilitated substrate entry via the carboxyl-end-first orientation, allowing dioxygenation to occur at positions closer to the carboxyl terminus in GLA, AA and DHA and altered the dioxygenation preference in ω-3 PUFAs from the ω-5 to the ω-2 position. Regioselectivity at the ω-2 position is novel in LOXs and offers advantages for producing long-chain ω-hydroxycarboxylic acids. The significant role of L445 in determining substrate preference, regioselectivity and substrate orientation in Bt-LOX, provide an incentive to investigate the effect of the corresponding residue in other LOXs. Modifying these key residues facilitates the synthesis of diverse FAHPs from various PUFAs, thus promoting the utilization of bacterial LOXs as environmentally friendly and sustainable biocatalysts in a wide range of applications.

Funding resource

The PhD study of R. Chrisnasari was supported by the Indonesian Endowment Fund for Education (LPDP, grant number 0006605/BIO/D/BUDI-2019).

CRediT authorship contribution statement

Tom A. Ewing: Writing – review & editing, Supervision, Conceptualization. **Willem J.H. van Berkel:** Writing – review & editing, Supervision. **Jean-Paul Vincken:** Writing – review & editing, Supervision. **Khoa A. Nguyen:** Writing – review & editing, Writing – original draft, Formal analysis. **Marie Hennebelle:** Writing – review & editing, Supervision, Conceptualization. **Ruth Chrisnasari:** Writing – review & editing, Writing – original draft, Visualization, Methodology, Investigation, Formal analysis, Conceptualization.

Declaration of Competing Interest

None.

Data availability

Data will be made available on request.

Acknowledgment

We extend our gratitude to Prof. Marco W. Fraaije and Dr. Hein J. Wijma from the University of Groningen for their contribution to generating the Alphafold2 model of Bt-LOX. Additionally, we express our appreciation to Mark Sanders, Dr. Roelant Hilgers, and Peter de Gijsel for their invaluable assistance during the development of the RP-UHPLC-PDA-HRMS method, and to Rene Kuijpers for his support during SEC analysis. Special thanks to Dylan Jetten for his role in developing the docking protocol for Bt-LOX. Part of the presented results was obtained using a Thermo Scientific Q Exactive Focus Orbitrap MS system, owned by Shared Research Facilities-WUR and subsidized by the province of Gelderland, The Netherlands.

Appendix A. Supporting information

Supplementary data associated with this article can be found in the online version at doi:10.1016/j.nbt.2024.09.007.

References

[1] Casey R, Hughes RK. Recombinant lipoxygenases and oxylipin metabolism in relation to food quality. Food Biotechnol 2004;18:135–70. https://doi.org/10.1081/FBT-200025673.
[2] Liu C, Liu F, Cai J, Xie UW, Long TE, Turner SR, et al. Polymers from fatty acids: Poly(co-hydroxyl tetradecanoic acid) synthesis and physico-mechanical studies. ACS Symp Ser 2012;1105:131–50. https://doi.org/10.1021/BK-2012-1105.CH009.
[3] Otte KB, Kittelberger J, Kirtz M, Nestl BM, Hauer B. Whole-cell one-pot biosynthesis of azelaic acid. ChemCatChem 2014;6:1003–9. https://doi.org/10.1002/cctc.201300787.
[4] Qi YK, Pan J, Zhang ZJ, Xu JH. Whole-cell one-pot biosynthesis of dodecanedioic acid from renewable linoleic acid. Bioresour Bioprocess 2024;11. https://doi.org/10.1186/s40643-024-00770-8.
[5] Coenen A, Ferrer M, Jaeger KE, Schörken U. Synthesis of 12-aminododecenoic acid by coupling transaminase to oxylipin pathway enzymes. Appl Microbiol Biotechnol 2023;107:2209–21. https://doi.org/10.1007/s00253-023-12422-6.
[6] An JU, Song YS, Kim KR, Ko YJ, Yoon DY, Oh DK. Biotransformation of polyunsaturated fatty acids to bioactive hepoxilins and trioxilins by microbial enzymes. Nat Commun 2018;9:1–10. https://doi.org/10.1038/s41467-017-02543-8.
[7] An JU, Kim SE, Oh DK. Molecular insights into lipoxygenases for biocatalytic synthesis of diverse lipid mediators. Prog Lipid Res 2021;83. https://doi.org/10.1016/j.plipres.2021.101110.
[8] Lee J, An J-U, Kim T-H, Ko Y-J, Park J-B, Oh D-K. Discovery and engineering of a microbial double-oxygenating lipoxygenase for synthesis of dihydroxy fatty acids as specialized pro-resolving mediators. ACS Sustain Chem Eng 2022;8:16172–83. https://doi.org/10.1021/acssuschemeng.0c04793.
[9] Ishihara T, Yoshida M, Arita M. Omega-3 fatty acid-derived mediators that control inflammation and tissue homeostasis. Int Immunol 2019;31:559–67. https://doi.org/10.1093/INTIMM/DXZ001.
[10] Basil MC, Levy BD. Specialized pro-resolving mediators: endogenous regulators of infection and inflammation. Nat Rev Immunol 2015 16:1 2015;16:51–67. https://doi.org/10.1038/NRI.2015.4.
[11] Qi Y-K, Zheng Y-C, Zhang Z-J, Xu J-H. Efficient transformation of linoleic acid into 13(*S*)-hydroxy-9,11-(*Z*,*E*)-octadecadienoic acid using putative lipoxygenases from Cyanobacteria. ACS Sustain Chem Eng 2020;8:5558–65. https://doi.org/10.1021/acssuschemeng.9b07457.
[12] Oh CW, Kim SE, Lee J, Oh DK. Bioconversion of C20- and C22-polyunsaturated fatty acids into 9*S*,15*S*- and 11*S*,17*S*-dihydroxy fatty acids by *Escherichia coli* expressing double-oxygenating 9*S*-lipoxygenase from *Sphingopyxis macrogoltabida*. J Biosci Bioeng 2022;134:14–20. https://doi.org/10.1016/J.JBIOSC.2022.04.001.
[13] Newie J, Andreou A, Neumann P, Einsle O, Feussner I, Ficner R. Crystal structure of a lipoxygenase from *Cyanothece* sp. may reveal novel features for substrate acquisition. J Lipid Res 2016;57:276–86. https://doi.org/10.1194/jlr.M064980.
[14] Ellamar JB, Kim IH, Hou CT, Park HS, Kim HR. Isolation and identification of a variant strain of *Pseudomonas aeruginosa* PR3 with enhanced production of 7,10-dihydroxy-8(*E*)-octadecenoic acid. Biocatal Agric Biotechnol 2019;18:101068. https://doi.org/10.1016/j.bcab.2019.101068.
[15] Goloshchapova K, Stehling S, Heydeck D, Blum M, Kuhn H. Functional characterization of a novel arachidonic acid 12*S*-lipoxygenase in the halotolerant bacterium *Myxococcus fulvus* exhibiting complex social living patterns. Microbiol Open 2018;8:1–17. https://doi.org/10.1002/mbo3.775.
[16] An JU, Hong SH, Oh DK. Regiospecificity of a novel bacterial lipoxygenase from *Myxococcus xanthus* for polyunsaturated fatty acids. Biochim Biophys Acta Mol Cell Biol Lipids 2018;1863:823–33. https://doi.org/10.1016/j.bbalip.2018.04.014.
[17] Banthiya S, Kalms J, Galemou Yoga E, Ivanov I, Carpena X, Hamberg M, et al. Structural and functional basis of phospholipid oxygenase activity of bacterial lipoxygenase from *Pseudomonas aeruginosa*. Biochim Biophys Acta Mol Cell Biol Lipids 2016;1861:1681–92. https://doi.org/10.1016/j.bbalip.2016.08.002.
[18] Kim SE, Lee J, An JU, Kim TH, Oh CW, Ko YJ, et al. Regioselectivity of an arachidonate 9*S*-lipoxygenase from *Sphingopyxis macrogoltabida* that biosynthesizes 9*S*,15*S*- and 11*S*,17*S*-dihydroxy fatty acids from C20 and C22 polyunsaturated fatty acids. Biochim Biophys Acta Mol Cell Biol Lipids 2022;1867:159091. https://doi.org/10.1016/J.BBALIP.2021.159091.
[19] Busquets M, Deroncelé V, Vidal-Mas J, Rodríguez E, Guerrero A, Manresa A. Isolation and characterization of a lipoxygenase from *Pseudomonas* 42A2 responsible for the biotransformation of oleic acid into (S)-(*E*)-10-hydroxy-8-octadecenoic acid. Antonie van Leeuwenhoek. Int J Gen Mol Microbiol 2004;85:129–39. https://doi.org/10.1023/B:ANTO.0000020152.15440.65.
[20] An JU, Kim BJ, Hong SH, Oh DK. Characterization of an omega-6 linoleate lipoxygenase from *Burkholderia thailandensis* and its application in the production of 13-hydroxyoctadecadienoic acid. Appl Microbiol Biotechnol 2015;99:5487–97. https://doi.org/10.1007/s00253-014-6353-8.

[21] Hughes RK, Wu Z, Robinson DS, Hardy D, West SI, Fairhurst SA, et al. Characterization of authentic recombinant pea-seed lipoxygenases with distinct properties and reaction mechanisms. Biochem J 1998;333:33–43. https://doi.org/10.1042/bj3330033.

[22] Chrisnasari R, Hennebelle M, Vincken J, Berkel WJH, Van, Ewing A. Bacterial lipoxygenases: Biochemical characteristics, molecular structure and potential applications. Biotechnol Adv 2022;61:108046. https://doi.org/10.1016/j.biotechadv.2022.108046.

[23] Gao B, Boeglin WE, Brash AR. Omega-3 fatty acids are oxygenated at the n-7 carbon by the lipoxygenase domain of a fusion protein in the cyanobacterium *Acaryochloris marina*. Biochim Biophys Acta Mol Cell Biol Lipids 2010;1801:58–63. https://doi.org/10.1016/J.BBALIP.2009.09.004.

[24] Andreou A, Vanko M, Bezakova L, Feussner I. Properties of a mini 9*R* -lipoxygenase from *Nostoc* sp. PCC 7120 and its mutant forms. Phytochemistry 2008;69:1832–7. https://doi.org/10.1016/j.phytochem.2008.03.002.

[25] Van Os CPA, Rijke-Schilder GPM, Van Halbeek H, Verhagen J, Vliegenthart JFG. Double dioxygenation of arachidonic acid by soybean lipoxygenase-1. Kinetics and regio-stereo specificities of the reaction steps. Biochim Et Biophys Acta Lipids Lipid Metab 1981;663:177–93. https://doi.org/10.1016/0005-2760(81)90204-6.

[26] Kim TH, Lee J, Kim SE, Oh DK. Biocatalytic synthesis of dihydroxy fatty acids as lipid mediators from polyunsaturated fatty acids by double dioxygenation of the microbial 12S-lipoxygenase. Biotechnol Bioeng 2021;118:3094–104. https://doi.org/10.1002/bit.27820.

[27] Vogel R, Jansen C, Roffeis J, Reddanna P, Forsell P, Claesson HE, et al. Applicability of the triad concept for the positional specificity of mammalian lipoxygenases. J Biol Chem 2010;285:5369–76. https://doi.org/10.1074/JBC.M109.057802.

[28] Newcomer ME, Brash AR. The structural basis for specificity in lipoxygenase catalysis. Protein Sci 2015;24:298–309. https://doi.org/10.1002/pro.2626.

[29] Sloane DL, Leung R, Sigal Cralk CS. E. A primary determinant for lipoxygenase positional specificity. Nature 1991;354:149. https://doi.org/10.1038/354149a0.

[30] Borngräber S, Kuban RJ, Anton M, Kühn H. Phenylalanine 353 is a primary determinant for the positional specificity of mammalian 15-lipoxygenases. J Mol Biol 1996;264:1145–53. https://doi.org/10.1006/jmbi.1996.0702.

[31] Borngräber S, Browner M, Gillmor S, Gerth C, Anton M, Fletterick R, et al. Shape and specificity in mammalian 15-lipoxygenase active site. The functional interplay of sequence determinants for the reaction specificity. J Biol Chem 1999;274:37345–50. https://doi.org/10.1074/JBC.274.52.37345.

[32] Coffa G, Brash AR. A single active site residue directs oxygenation stereospecificity in lipoxygenases: Stereo control is linked to the position of oxygenation. Proc Natl Acad Sci USA 2004;101:15579–84. https://doi.org/10.1073/pnas.0406727101.

[33] Kalms J, Banthiya S, Galemou Yoga E, Hamberg M, Holzhutter HG, Kuhn H, et al. The crystal structure of *Pseudomonas aeruginosa* lipoxygenase Ala420Gly mutant explains the improved oxygen affinity and the altered reaction specificity. Biochim Biophys Acta Mol Cell Biol Lipids 2017;1862:463–73. https://doi.org/10.1016/j.bbalip.2017.01.003.

[34] Sim DH, Shin KC, Oh DK. 13-Hydroxy-9Z,11E-octadecadienoic acid production by recombinant cells expressing *Burkholderia thailandensis* 13-lipoxygenase. JAOCS 2015;92:1259–66. https://doi.org/10.1007/s11746-015-2694-4.

[35] Nezhad NG, Rahman RNZRA, Normi YM, Oslan SN, Shariff FM, Leow TC. Recent advances in simultaneous thermostability-activity improvement of industrial enzymes through structure modification. Int J Biol Macromol 2023;232:123440. https://doi.org/10.1016/j.ijbiomac.2023.123440.

[36] Zhang YY, Radmark O, Samuelsson B. Mutagenesis of some conserved residues in human 5-lipoxygenase: Effects on enzyme activity (leukotrienes/eicosanoids/arachidonic acid/dioxygenase). PNAS 1992;89:485–9. https://doi.org/10.1073/pnas.89.2.48.

[37] Bradford MM. A rapid and sensitive method for the quantitation of microgram quantities of protein utilizing the principle of protein-dye binding. Anal Biochem 1976;72:248–54.

[38] Westphal AH, van Berkel WJH. Techniques for enzyme purification. In: de Gonzalo G, Lavandera I, editors. Biocatalysis for practitioners: techniques, reactions and applications. 1st ed., Weinheim. Wiley-VCH; 2021. p. 3–31. https://doi.org/10.1002/9783527824465.ch1.

[39] Axelrod B, Cheesbrough TM, Laakso S. Lipoxygenase from soybeans: EC 1.13.11.12 linoleate: oxygen oxidoreductase. Methods Enzymol 1981;71:441–51. https://doi.org/10.1016/0076-6879(81)71055-3.

[40] Chrisnasari R, Ewing TA, Hilgers R, van Berkel WJH, Vincken J-P, Hennebelle M. Versatile ferrous oxidation–xylenol orange assay for high-throughput screening of lipoxygenase activity. Appl Microbiol Biotechnol 2024;108:266. https://doi.org/10.1007/s00253-024-13095-5.

[41] Jumper J, Evans R, Pritzel A, Green T, Figurnov M, Ronneberger O, et al. Highly accurate protein structure prediction with AlphaFold. Nature 2021;596:583–9. https://doi.org/10.1038/S41586-021-03819-2.

[42] Waterhouse AM, Procter JB, Martin DMA, Clamp M, Barton GJ. Sequence analysis Jalview Version 2-a multiple sequence alignment editor and analysis workbench. Bioinfomatics Appl Note 2009;25:1189–91. https://doi.org/10.1093/bioinformatics/btp033.

[43] Niklasson M, Andresen C, Helander S, Roth MGL, Zimdahl Kahlin A, Lindqvist Appell M, et al. Robust and convenient analysis of protein thermal and chemical stability. Protein Sci 2015;24:2055–62. https://doi.org/10.1002/pro.2809.

[44] Greenfield NJ. Using circular dichroism collected as a function of temperature to determine the thermodynamics of protein unfolding and binding interactions. Nat Protoc 2007;1:2527–35. https://doi.org/10.1038/nprot.2006.204.

[45] van Boekel MAJS. Kinetics of protein and enzyme denaturation. Kinetic Modeling of Reactions in Foods. 1st edition.,. Boca Raton: CRC Press,; 2008. https://doi.org/10.1201/9781420017410.

[46] Corongiu FP. Bani S. Detection of conjugated dienes by second derivative ultraviolet spectrophotometry. Methods Enzym 1941;vol. 233:303–10. https://doi.org/10.1016/s0076-6879(94)33033-6.

[47] Derogis PBMC, Chaves-Fillho AB, Miyamoto S. Characterization of hydroxy and hydroperoxy polyunsaturated fatty acids by mass spectrometry. Adv Exp Med Biol, vol. 1127. Springer New York LLC,; 2019. p. 21–35. https://doi.org/10.1007/978-3-030-11488-6_2.

[48] Derogis PBMC, Freitas FP, Marques ASF, Cunha D, Appolinário PP. Lipidomic analysis. PLoS One 2013;8:77561. https://doi.org/10.1371/journal.pone.0077561.

[49] Ali MH, Imperiali B. Protein oligomerization: how and why. Bioorg Med Chem 2005;13:5013–20. https://doi.org/10.1016/j.bmc.2005.05.037.

[50] Kumari N, Yadav S. Modulation of protein oligomerization: An overview. Prog Biophys Mol Biol 2019;149:99–113. https://doi.org/10.1016/j.pbiomolbio.2019.03.003.

[51] Andreou A, Göbel C, Hamberg M, Feussner I. A bisallylic mini-lipoxygenase from cyanobacterium *Cyanothece* sp. that has an iron as cofactor. J Biol Chem 2010;285:14178–86. https://doi.org/10.1074/jbc.M109.094771.

[52] Deschamps JD, Ogunsola AF, Jameson JB, Yasgar A, Flitter BA, Freedman CJ, et al. Biochemical and cellular characterization and inhibitor discovery of *Pseudomonas aeruginosa* 15-lipoxygenase. Biochemistry 2016;55:3329–40. https://doi.org/10.1021/acs.biochem.6b00338.

[53] Bae JH, Kim DS, Suh MJ, Oh SR, Lee IJ, Kang SC, et al. Production and identification of a novel compound, 7,10-dihydroxy-8(*E*)-hexadecenoic acid from palmitoleic acid by *Pseudomonas aeruginosa* PR3. Appl Microbiol Biotechnol 2007;75:435–40. https://doi.org/10.1007/s00253-006-0832-5.

[54] Newie J, Neumann P, Werner M, Mata RA, Ficner R, Feussner I. Lipoxygenase 2 from *Cyanothece* sp. controls dioxygen insertion by steric shielding and substrate fixation. Sci Rep 2017 7:1 2017;7:1–12. https://doi.org/10.1038/s41598-017-02153-w.

[55] Bae JH, Hou CT, Kim HR. Thermostable lipoxygenase is a key enzyme in the conversion of linoleic acid to trihydroxy-octadecenoic acid by *Pseudomonas aeruginosa* PR3. Biotechnol Bioprocess Eng 2010;15:1022–30. https://doi.org/10.1007/s12257-010-0273-y.

[56] Lu X, Zhang J, Liu S, Zhang D, Xu Z, Wu J, et al. Overproduction, purification, and characterization of extracellular lipoxygenase of *Pseudomonas aeruginosa* in *Escherichia coli*. Appl Microbiol Biotechnol 2013;97:5793–800. https://doi.org/10.1007/s00253-012-4457-6.

[57] Yi J-J, Heo S-Y, Ju J-H, Oh B-R, Son WS, Seo J-W. Synthesis of 13*R*,20-dihydroxydocosahexaenoic acid by site-directed mutagenesis of lipoxygenase derived from *Oscillatoria nigro-viridis* PCC 7112. Biochem Biophys Res Commun 2020;533:893–8. https://doi.org/10.1016/j.bbrc.2020.09.079.

[58] Zheng Y, Boeglin WE, Schneider C, Brash AR. A 49-kDa mini-lipoxygenase from *Anabaena* sp. PCC 7120 retains catalytically complete functionality. J Biol Chem 2008;283:5138–47. https://doi.org/10.1074/jbc.M705780200.

[59] Grechkin AN, Hamberg M. The "heterolytic hydroperoxide lyase" is an isomerase producing a short-lived fatty acid hemiacetal. Biochim Biophys Acta Mol Cell Biol Lipids 2004;1636:47–58. https://doi.org/10.1016/j.bbalip.2003.12.003.

[60] Grechkin AN, Brühlmann F, Mukhtarova LS, Gogolev YV, Hamberg M. Hydroperoxide lyases (CYP74C and CYP74B) catalyze the homolytic isomerization of fatty acid hydroperoxides into hemiacetals. Biochim Biophys Acta Mol Cell Biol Lipids 2006;1761:1419–28. https://doi.org/10.1016/j.bbalip.2006.09.002.

[61] Björkhem I. On the role of alcohol dehydrogenase in ω-oxidation of fatty acids. Eur J Biochem 1972;30:441–51. https://doi.org/10.1111/j.1432-1033.1972.tb02116.x.

[62] Gardner HW. Oxygen radical chemistry of polyunsaturated fatty acids. Free Radic Biol Med 1989;7:65–86. https://doi.org/10.1016/0891-5849(89)90102-0.

[63] Gardner HW, Plattner RD. Linoleate hydroperoxides are cleaved heterolytically into aldehydes by a Lewis acid in aprotic solvent. Lipids 1984;19:294–9. https://doi.org/10.1007/BF02534458.

[64] Song JW, Jeon EY, Song DH, Jang HY, Bornscheuer UT, Oh DK, et al. Multistep enzymatic synthesis of long-chain α,ω-dicarboxylic and ω-hydroxycarboxylic acids from renewable fatty acids and plant oils. Angew Chem Int Ed 2013;52:2534–7. https://doi.org/10.1002/anie.201209187.

[65] Seo J-H, Lee S-M, Lee J, Park J-B. Adding value to plant oils and fatty acids: Biological transformation of fatty acids into-hydroxycarboxylic,-dicarboxylic, and-aminocarboxylic acids. J Biotechnol 2015;216:158–66. https://doi.org/10.1016/j.jbiotec.2015.10.024.